Organic Matter Export Rates and the Pathways of Nutrient Supply in the Ocean

Paul Quay[1] (iD)

[1]School of Oceanography, University of Washington, Seattle, WA, USA

Abstract Multiyear estimates of organic matter (OM) export based primarily on oxygen and dissolved inorganic carbon surface layer budgets applied basin-wide for the Pacific, Atlantic, and S. Indian Oceans yield an inter-basin range from 1 to 3 mol C/m²/yr with a global mean of 2.0 mol C/m²/yr (8.5 Gt C/yr). OM export rates per area in the Pacific and Atlantic oceans are twice than that in the Indian Ocean. The supply of nutrients from the Southern Ocean can potentially support ∼70% of the observed OM export in the ocean based on observed surface current velocities and PO_4 distributions. Horizontal flux of PO_4 and dissolved organic phosphorous in the surface layer can support ∼50%, 20%, and 15% of observed OM export in the Pacific, S. Indian and Atlantic oceans, respectively, with the remainder being supplied vertically from the subsurface. Potential utilization of unused surface PO_4 in the subtropical gyre yields ∼0.1 mol C/m²/yr increase in OM export in the Pacific and Atlantic oceans but a ∼0.8 mol C/m²/yr increase in the S. Indian ocean suggesting that stronger nutrient limitation contributes to lower export rates observed in the Indian ocean.

Plain Language Summary A small fraction of the organic matter (OM) produced photosynthetically by phytoplankton in the surface ocean is transferred (exported) to deeper portions of the ocean. The rate at which the OM is exported to the subsurface ocean has a significant impact on the ocean's concentrations of dissolved carbon dioxide and oxygen gases. New estimates of the OM export rate per unit area for the Atlantic, Pacific, and Indian oceans are presented based on surface layer oxygen and carbon dioxide budgets. The OM export rate is similar for the Atlantic and Pacific oceans but twice the rate in the Indian ocean. Most of the dissolved nutrients needed by phytoplankton to produce OM originate on the surface of the Southern Ocean (south of 50°S) and are transported via circulation to all the ocean basins where they are consumed by phytoplankton. Between ∼15 and 50% of the nutrients are supplied via surface currents, whereas the remainder is supplied via mixing from the subsurface layers of the ocean.

1. Introduction

The transfer or export of organic matter (OM) produced in the surface layer of the ocean to deeper layers in the ocean can sequester carbon (CO_2) from the atmosphere for decades to centuries (e.g., DeVries & Weber, 2017). The degradation of this OM in the thermocline and deep sea consumes oxygen (O_2) and affects the extent of oxygen minimum zones. Despite the fundamentally important role of OM export in the ocean carbon and oxygen cycles, there is a notable scarcity of observation-based estimates of export over basin-wide and multiyear time scales. Currently, our knowledge of global patterns of OM export relies mostly on model- and satellite-based estimates, which yield global ocean export that varies threefold from ∼5 to 13 Pg C/yr (e.g., Emerson, 2014; Li & Cassar, 2016). This level of uncertainty affects our ability to accurately determine the role of the biological pump in sequestering CO_2 in today's ocean and its impact on future atmospheric CO_2 levels. Furthermore, our understanding of the processes supplying the nutrients that fuel OM export is uncertain, especially for the subtropical gyres.

Regional and temporal variations of OM export in the ocean are potentially significant because the characteristics of the ocean's ecosystem that impact export vary markedly across the ocean's biomes, for example, primary production rates (PP), plankton size and elemental composition, zooplankton grazing and vertical migration rates, dissolved organic matter (DOM) production, etc. (e.g., Boyd & Trull, 2007). Models typically predict a response to climate change that yields large variations in regional export rates (±40%) but much less variation in global export (±8%) (e.g., Laufkötter et al., 2013), which implies that factors controlling OM export vary substantially on regional scales but global ocean response is more modest because changes in one region are offset by opposite changes in another region.

Our best understanding of interannual variability and long-term mean state of OM export comes from ocean time series sites where estimates of annual export determined by surface ocean O_2, nutrient, CO_2 mass balances are 3.0 ± 1.0, 3.3 ± 1.0, 2.5 ± 0.7, and 2.3 ± 0.6 mol C/m²/d at Bermuda (BATS), Canary Islands (ESTOC), Hawaii (ALOHA), and Ocean Station Papa (OSP), respectively (Emerson, 2014; Fawcett et al., 2018; Neuer et al., 2007). Over the last few years there has been a substantial increase in annual export rates estimated based on surface layer budgets of O_2, nitrate and CO_2 measured autonomously by floats, gliders, moorings (e.g., Arteaga et al., 2019; Billheimer et al., 2021; Bushinsky & Emerson, 2015; Fassbender et al., 2016; Yang et al., 2019) and by container ships for repeated basin-wide surveying (e.g., Ostle et al., 2015; Palevsky et al., 2016). Estimates of OM export based on sediment trap collection of sinking particles are typically substantially lower than export estimates based on surface layer budgets (Emerson, 2014) and, in part, due to the importance of DOM transport and zooplankton excretion as export pathways (e.g., Hansell & Carlson, 2001; Steinberg & Landry, 2017).

Here, new estimates of multi-year OM export for the Pacific, Atlantic and Indian ocean basins are presented based on surface layer O_2 and dissolved inorganic carbon (DIC) budgets. There are two goals of this work. First, to determine the spatial variability of OM export within and between each ocean basin. Second, to determine the pathways of dissolved nutrient supply that support OM export in each basin. Several features stand out. Basin-wide mean OM export in the Atlantic (2.6 ± 0.9 mol C/m²/yr) and Pacific (2.1 ± 0.8 mol C/m²/yr) are ~2-fold greater than in the S. Indian Ocean (0.9 ± 0.8 mol C/m²/yr) and together yield an ocean-wide mean of 2.0 ± 0.8 mol C/m²/yr (8.5 ± 3.4 Gt C/yr). The lowest OM export rates occur in the subtropical gyres of the S. Indian and S. Pacific oceans at ~1 mol C/m²/yr with the highest rates in the Equatorial Pacific and N. Atlantic (~3 mol C/m²/yr). Dissolved PO_4 originating in the surface layer of the Southern Ocean potentially supports ~$70 \pm 38\%$ of global OM export north of 50°S. Surface advective flux of dissolved PO_4 and organic phosphorous (DOP) potentially support ~50% of OM export in the Pacific and ≤20% in the Atlantic and Indian basins, which implies that the remaining portions are a result of vertical nutrient supply. The low OM export rate observed in the S. Indian Ocean appears to be, in part, a result of stronger limitations on dissolved P utilization.

2. Methods

Estimates of OM export based on surface layer budgets (e.g., O_2, CO_2, NO_3, PO_4) have the advantages of integrating over annual cycles and accounting for all pathways of OM export (e.g., particle sinking, transport of DOM, zooplankton vertical migration and excretion, etc.). The depth to which one integrates the surface layer budget is important as the degradation of particles and DOM decrease the OM export flux with increasing depth (Palevsky & Doney, 2018). A useful horizon for integration is the depth of the winter mixed layer because only OM export that passes this depth horizon removes CO_2 and nutrients from the surface ocean over the annual cycle. Several studies have shown that in the subpolar ocean, a significant portion (~40–90%) of the OM exported during the summer is degraded to dissolved nutrients which are returned to the mixed layer during winter (Kortzinger et al., 2008; Palevsky & Quay, 2017). Here, surface layer budgets of O_2 and DIC are used to estimate OM export as these methods have been used in the past and have been shown to yield consistent estimates of annual OM export (e.g., Quay et al., 2020; Yang et al., 2019). In the equatorial ocean, a surface PO_4 budget is used to estimate OM export. Here, budget-based export represents the OM that leaves the surface layer which at steady-state should be equivalent to net community respiration (gross production minus total respiration). Although most of the OM will be exported to depth, some may be exported as DOM horizontally to other regions of the surface ocean near the equator (Primeau et al., 2013).

2.1. O_2 Budget Approach to Estimate OM Export

The OM export rate (mol C/m²/yr) can be estimated from a surface layer O_2 budget, which is expressed as follows:

$$Z^* dO_2/dt = \text{Gas}_o + \text{Export}_o + \text{Supply}_o \tag{1}$$

Where Z equals the depth of the surface layer, t is time, Gas_o represents the net air-sea flux of O_2, which depends on the O_2 supersaturation (i.e., measured O_2 concentration minus the O_2 concentration expected in equilibrium with atmosphere) and gas transfer velocity, Export_o represents the O_2 produced photosynthetically by exported OM and Supply_o represents the input or loss of dissolved O_2 resulting from advection, mixing, eddies, etc. The Gas and Export terms usually dominate the O_2 budget although, as discussed below, in regions of significant

upwelling (equatorial ocean) and/or deep winter time mixing (Southern Ocean, subpolar N. Atlantic) the supply of O_2 undersaturated water from below can dominate. The O_2 budget was solved at monthly intervals because both Gas and Supply terms can vary significantly over the annual cycle (e.g., Bushinsky & Emerson, 2015). The O_2 gas transfer rate, including bubble injection, was determined following the procedure of Yang et al. (2017). Surface O_2 supersaturation was determined from the World Ocean Atlas (WOA) monthly climatological data compilation (mean, standard error of mean, number of observations) at 5° latitude by 5° longitude resolution (Boyer et al., 2018). A comparison of the annual cycle of surface O_2 supersaturation determined from WOA data to a decade long average cycle measured at ALOHA, OSP, and BATS shows good agreement at OSP and BATS although with higher summertime O_2 saturation at ALOHA which also occurs using the GOSHIP-based GLODAP O_2 data set (Figure S1 in Supporting Information S1).

The WOA-based O_2 supersaturation data were averaged zonally across the width of the basin with each 5° latitude band containing an average of 1,300, 1,600, and 700 measurements for the Pacific, Atlantic and Indian oceans (~60–130 per month). To calculate OM export from the O_2 supersaturation data, it is assumed that any long-term time change in O_2 concentration and net horizontal O_2 transport for each basin-wide 5° latitude band integrated over the annual cycle are negligible relative to the air-sea O_2 flux based on this climatological data set. This assumption has been used previously when OM export was determined from O_2 budget based on long-term O_2 data collected during the CARINA program in N. Atlantic (Quay et al., 2020). At Stn ALOHA, where a monthly high-quality O_2 measurement record exists between 1990 and 2020, the measured surface O_2 concentrations have decreased by only 0.03 ± 0.03 µmol kg^{-1} per year (equivalent to -0.003 mol O_2/m^2/yr). Because the O_2 concentration typically decreases with depth below the winter mixed layer, vertical mixing yields a net O_2 loss from the surface layer over the annual cycle. Yang et al. (2017) determined the magnitude of this flux by estimating the turbulent mixing rate (Kz) and measured O_2 gradients from ARGO floats and found that accounting for the O_2 flux out the base of the mixed layer increased the estimated export rate by ~10%. Here, this vertical O_2 flux was estimated using the Kz values determined by Yang et al. and the O_2 depth gradient from the WOA data base, which yielded a downward O_2 flux that increased the estimated export rate by 2%, 6%, and 14% for the Indian, Atlantic and Pacific basins, respectively. The net organic carbon export rate equals the sum of the air-sea and vertical diffusive O_2 fluxes divided by the (O/C) of the exported OM, which is assumed at 1.45 (Hedges et al., 2002).

The error in OM export estimated from O_2 budget was based on the errors in the mean O_2 supersaturation and air-sea O_2 gas transfer rate. The standard errors in the mean surface O_2 saturation at $5° \times 5°$ grid have been compiled by WOA. The error in the diffusive O_2 gas transfer rate is assumed to be $\pm25\%$ and error in the bubble transfer rates is assumed to be $\pm10\%$ and the error in the vertical O_2 flux at the base of the mixed layer was assumed to be $\pm50\%$ following Yang et al. (2017). The overall uncertainty in the O_2 budget-based export was estimated for each 5° latitude band zonally averaged across each basin, which yielded a mean uncertainty of $53 \pm 14\%$ which agrees with the error of $\pm50\%$ reported by Yang et al. (2017). As a test of the O_2 budget approach, estimates of OM export based on the measured annual cycles in surface O_2 supersaturation at ALOHA, OSP, and BATS (Figure S1 in Supporting Information S1) were determined at 2.0 ± 1.1, 2.7 ± 1.1, and 2.7 ± 1.2 mol C/m^2/yr, respectively, which all fall within the range of previous estimates for these three sites, presented above.

There are some clear regional patterns in the annual mean O_2 supersaturation in the surface layer (Figure 1). The highest O_2 supersaturations are found in the N. Atlantic and lowest O_2 supersaturations are found in the Southern Ocean (south of 55°S). O_2 supersaturation in the northern basins of the Atlantic and Pacific oceans is slightly higher than in the southern basins. There is an O_2 supersaturation minimum near the equator, which yields negative supersaturation values in the Pacific but not in the Atlantic and Indian oceans. Negative O_2 supersaturation in the surface layer occurs when either in situ rates of community respiration exceed primary production (NCP < 0) or when the rate of subsurface O_2 depleted waters being upwelled or mixed into the surface layer exceeds the rate of O_2 production from NCP. There is a clear seasonal cycle in surface O_2 saturation at polar latitudes (>50°) with summertime maximum up to 6% and wintertime minimum at negative supersaturations down to -6% (Figure S2 in Supporting Information S1). As a result, OM export rates based on the summertime drawdown of DIC, NO_3, or PO_4 can significantly overestimate the annual OM export rate in regions with deep winter mixed layers (e.g., Kortzinger et al., 2008; Palevsky & Quay, 2017). Similarly, near the equator upwelling of O_2 depleted subsurface water lowers surface O_2 supersaturation (Figure 1; Figure S2 in Supporting Information S1). Thus, in regions poleward of ~50° or within 5° of the equator where the input of subsurface O_2 depleted water is significant relative to air-sea O_2 exchange, the O_2 budget approach was not used to estimate annual OM export.
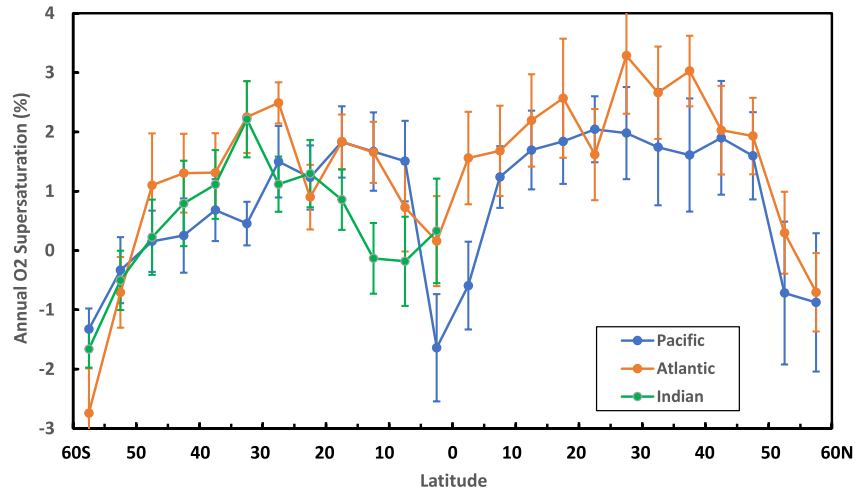
Figure 1. Annual mean surface O_2 supersaturation (observed saturation (%)—100) averaged zonally across the basin and over 5° latitude bands based on 2018 World Ocean Atlas (WOA) monthly data compilation. Error bars represent the average standard error of O_2 saturation compiled by WOA.

2.2. DIC + DIC^{13} Budget Approach to Estimate OM Export

A combination of surface layer DIC and DIC^{13} budgets has been used at many locations to estimate the OM export rate (e.g., Gruber et al., 2002; Quay et al., 2009; Yang et al., 2019; Zhang & Quay, 1997). The DIC and DIC^{13} budget expressions are similar to those for the O_2 budget as follows:

$$Z^* d\text{DIC}/dt = \text{Gas}_c - \text{Export}_c + \text{Supply}_c \tag{2}$$

$$Z^* d\left[\text{DIC}^*(^{13}\text{C}/^{12}\text{C})\right]/dt = \text{Gas}_c{}^*(^{13}\text{C}/^{12}\text{C})_{\text{gas}} - \text{Export}_c{}^*(^{13}\text{C}/^{12}\text{C})_{\text{exp}} + \text{Supply}_c{}^*(^{13}\text{C}/^{12}\text{C})_{\text{supp}} \tag{3}$$

Gas_c represents the air-sea flux of CO_2, Export_c represents the organic carbon export rate and Supply_c represents the input or loss of DIC resulting from advection, mixing, eddies etc. $(^{13}\text{C}/^{12}\text{C})_{\text{gas}}$ represents the ratio of the air-sea $^{13}CO_2$ to CO_2 gas flux, $(^{13}\text{C}/^{12}\text{C})_{\text{exp}}$ represents the $^{13}\text{C}/^{12}\text{C}$ of OM being exported and $(^{13}\text{C}/^{12}\text{C})_{\text{supp}}$ represents the ratio of the DIC^{13}/DIC being supplied by physical processes. Gas_c is estimated from climatological surface ΔpCO_2 observations by Takahashi et al. (2009) and CO_2 gas transfer rates (Wanninkhof, 2014) estimated from CCMP winds (Atlas et al., 2011). $(^{13}\text{C}/^{12}\text{C})_{\text{gas}}$ depends on the air-sea gradients of dissolved CO_2 and the $^{13}\text{C}/^{12}\text{C}$ of the dissolved CO_2 (Quay et al., 2009). $(^{13}\text{C}/^{12}\text{C})_{\text{exp}}$ is estimated from the compilation of $^{13}\text{C}/^{12}\text{C}$ measurement of particles in the surface ocean (Goericke & Fry, 1994). $(^{13}\text{C}/^{12}\text{C})_{\text{supp}}$ represents the ratio of depth gradients of DIC and DIC^{13} (i.e., DIC^{13} = DIC$^*(^{13}\text{C}/^{12}\text{C})_{\text{DIC}}$) in the upper 300 m of the water column and the ratio of surface layer horizontal gradients of DIC and DIC^{13} determined by regression assuming that the supply of DIC is evenly divided (50 ± 25%) between horizontal surface transport and vertical mixing, as discussed below. The GLODAP data compilation of DIC and $^{13}\text{C}/^{12}\text{C}$ of DIC observations (Key et al., 2015) is used to determine the $(^{13}\text{C}/^{12}\text{C})_{\text{gas}}$ and $(^{13}\text{C}/^{12}\text{C})_{\text{supp}}$ with data being averaged zonally across the basin and over 5° latitude bins.

Combining the DIC and DIC^{13} budgets and estimating Gas_c and $(^{13}\text{C}/^{12}\text{C})_{\text{gas}}$ from ocean-wide data sets of ΔpCO_2 and $^{13}\text{C}/^{12}\text{C}$ of DIC yields an estimate of the OM export rate using the following expression:

$$\begin{aligned}\text{OM export} = &\left[\text{Gas}_c{}^*\left[(^{13}\text{C}/^{12}\text{C})_{\text{gas}} - (^{13}\text{C}/^{12}\text{C})_{\text{supp}}\right] - Z^* d\text{DIC}^{13}/dt + Z^* d\text{DIC}/dt^*(^{13}\text{C}/^{12}\text{C})_{\text{supp}}\right] \\ &/\left[(^{13}\text{C}/^{12}\text{C})_{\text{exp}} - (^{13}\text{C}/^{12}\text{C})_{\text{supp}}\right]\end{aligned} \tag{4}$$

The dDIC/dt and dDIC^{13}/dt terms in Equation 4 represent the long term (decadal) changes resulting from anthropogenic CO_2 uptake (e.g., Quay et al., 2017). A recent comparison of OM export rates determined from the O_2 budget and DIC + DIC^{13} budget approaches showed good agreement at subtropical sites in the Atlantic, Pacific and Indian Oceans (Yang et al., 2019). DIC + DIC^{13} budget approach has the least error in calculated export term in regions where air-sea CO_2 gas exchange yields a decrease in the $^{13}\text{C}/^{12}\text{C}$ of DIC that is offset by the increase in the $^{13}\text{C}/^{12}\text{C}$ of DIC resulting from the export of ^{13}C-depleted organic carbon. This situation occurs between

~50°S and 50°N (Figure S3 in Supporting Information S1). In contrast, poleward of ~50° air-sea CO_2 exchange increases the $^{13}C/^{12}C$-DIC (Figure S3 in Supporting Information S1) and under these conditions the supply of ^{13}C depleted DIC by physical processes offsets the $^{13}C/^{12}C$ increases due to both air-sea CO_2 exchange and organic carbon export, which causes significant errors (≥100%) in the calculated OC export. As a result, DIC + DIC^{13} based estimates of OM export poleward of 50° are excluded from this analysis. Near the equator, the upwelling of subsurface water with high pCO_2 and ^{13}C depleted DIC can dominate over air-sea CO_2 and $^{13}CO_2$ flux (Quay et al., 2009) ; thus, DIC + DIC^{13} budget-based estimates of OM export equatorward of 5° are excluded from this analysis. The consistency of the latitudinal pattern in the air-sea $^{13}CO_2$ disequilibrium for the Pacific, Atlantic and Indian oceans (Figure S3 in Supporting Information S1) highlights an important characteristic of the DIC + DIC^{13} budget approach, that is, the $^{13}C/^{12}C$ of DIC in the surface layer in regions of the ocean equatorward of 50° shows little seasonal and zonal variability. As a result, relatively few measurements yield an accurate estimate of the surface $^{13}C/^{12}C$ of DIC. Because the equilibration time of the $^{13}C/^{12}C$ of DIC to air-sea CO_2 exchange is slow (~10 years) and the $(^{13}C/^{12}C)_{supp}$ represents long-term (multiyear) conditions, the OM export rate estimated from the DIC + DIC^{13} budget approach represents a long-term (climatological) mean. Note that the DIC + DIC^{13} approach yields an estimate of the DIC supply rate in addition to the export rate, which differs from the O_2 budget approach (Quay et al., 2009).

The error in the DIC + DIC^{13} budget-based estimate of OM export was determined using a Monte Carlo approach. The overall error depends primarily on the uncertainties in the air-sea CO_2 gas transfer rate, $(^{13}C/^{12}C)_{supp}$ and fraction of DIC supplied vertically and horizontally (50 ± 25%). Errors were determined over 5° latitude bands averaged across the width of each basin and yielded an average error of 53% for all basins.

2.3. PO$_4$ Budget Approach to Estimate OM Export

To estimate the OM export rate in the equatorial regions where there are issues with the O_2 and DIC + DIC^{13} budget approaches, as discussed above, a PO$_4$ budget approach is utilized. A surface layer PO$_4$ budget applied in the equatorial region takes advantage of the significant difference between the concentrations of dissolved PO$_4$ in upwelling water and surface water and assumes that upwelling of PO$_4$ dominates over labile DOP as the dissolved P source. The poleward volume divergence of water in the surface mixed layer is assumed to balance upwelling. In addition to the upwelling term, which dominates the surface PO$_4$ budget, poleward PO$_4$ resulting from eddy mixing were included in the PO$_4$ budget, as discussed below. OM export is determined using the following expression:

$$\text{OM export} = \left[\text{Meridional Volume Transport}^*(PO_{4z} - PO_{4o}) - A_x^* \text{Eddy Mixing}^*(\Delta PO_{4o}/\Delta y)\right] / \text{Surface Area}^*(C/P)_{exp} \quad (5)$$

Where z is upwelling depth, o is surface, A_x represents the cross-section area (basin width*surface layer depth), Δy is meridional distance, and $(C/P)_{exp}$ represents the C/P of exported OM, which is assumed to be 125 based on Martiny et al. (2013) compilation of suspended particles in the equatorial ocean. The poleward boundaries were set at 8°S and 8°N to avoid the impact of the off equator downwelling and equatorward convergence that occurs between ~5°S and 5°N (Johnson et al., 2001). Poleward volume transport at 8°S and 8°N were estimated from a climatological compilation of surface drifter velocities (Laurindo et al., 2017) integrated across the width of the basin (Figure 2) and climatological annually averaged mixed layer depth from ARGO (Holte et al., 2017). A horizontal surface eddy diffusivity of 10^4 m^2/s in the equatorial region (Roach et al., 2018) was assumed to estimate eddy mixing based surface PO$_4$ flux, which was less than 10% of the upwelling PO$_4$ flux in all basins. PO$_4$ concentrations were based on GLODAP 2016 gridded data compilation (1972–2013) at 1° × 1° resolution (Lauvset et al., 2016). The PO$_4$ concentrations in the upwelled water were taken at the depth of maximum upwelling (~60–70 m) (Johnson et al., 2001), which approximates the winter mixed layer depth at the equator. The equatorial PO$_4$ budgets presented here represent basin-wide averages while acknowledging that there may be significant zonal variations in OM export along the equator, especially in the Pacific where there is an east-west gradient in surface PO$_4$ concentrations that is not observed in the equatorial Atlantic and Indian basins.

2.4. Estimating Surface Supply Rates of PO$_4$ and DOP

To determine the importance of surface nutrient supply to support OM export, the surface advective PO$_4$ and DOP fluxes were determined based on surface velocities derived from drifter observations, which are considered
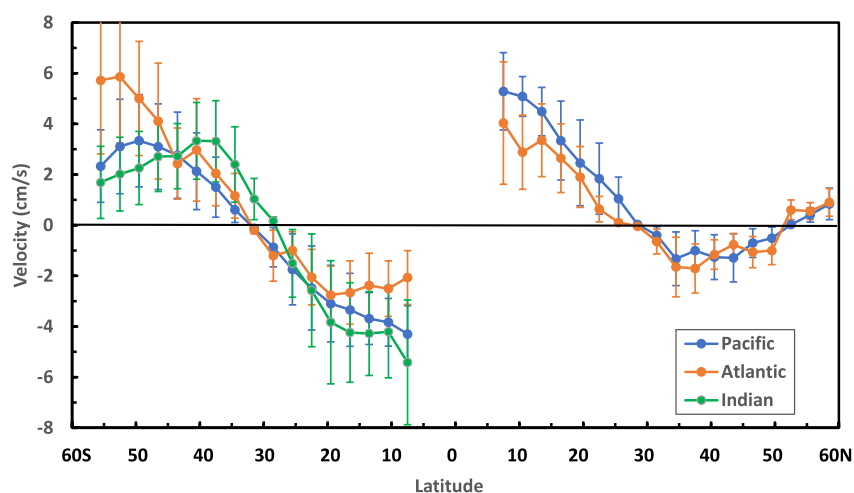
Figure 2. Meridional surface velocities (+ = northward) and standard errors based on climatological surface drifters (Laurindo et al., 2017) averaged zonally across the basin and over 3° latitude bands.

to provide accurate estimates of surface velocities on global scales (Laurindo et al., 2017) and compilations of surface PO_4 concentrations from GLODAP (Lauvset et al., 2016) and DOP (Knapp et al., 2021). In the subtropical gyres where surface PO_4 concentrations can reach low levels (<0.01 μM), the PO_4 data set of Martiny et al. (2019) based on high sensitivity detection methods is used. In subtropical regions where low-level PO_4 data are unavailable PO_4 is estimated from the GLODAP PO_4 data, which have been corrected for the offset from low-level PO_4 data of Martiny et al. (2019) (Figure S4 in Supporting Information S1).

The climatological surface advective PO_4 and DOP fluxes were determined using the observed global distributions of surface velocities from drifters (V) and mean annual mixed layer depth (Z) determined from ARGO floats.

$$PO_4 \text{ (or DOP) flux} = V * Z * PO_4 \text{ (or DOP) concentration} \qquad (6)$$

Meridional PO_4 and DOP fluxes were averaged over 10° longitude × 3° latitude intervals and integrated zonally across the basin, excluding the coastal zones. Zonal PO_4 and DOP fluxes were determined at the eastern and western basin boundaries at 3° latitude intervals. In the Indian Ocean, there was insufficient DOP data (Knapp et al., 2021) to estimate surface advective transport of DOP and advective surface PO_4 transport was not determined north of the equator because of the dominance of seasonal variations in monsoon-driven circulation and biological productivity. The PO_4 and DOP flux resulting from eddy mixing was added to the advective PO_4 transport in regions of high eddy activity, that is, at the northern boundary of the Antarctic Circumpolar Current (~50°S) and near the equator (8°S and N), assuming a horizontal eddy diffusivity of 10^4 m²/s (Roach et al., 2018). Surface DOP transport was negligible compared to PO_4 transport poleward of ~40° but significant within the equatorial and subtropical regions. Uncertainties in the surface advective PO_4 and DOP transport rates are primarily a result of errors in the drifter velocities, which have been compiled by Laurindo et al. (2017).

To determine the OM export (mol C/m²/yr) potentially supported by advective PO_4 and DOP fluxes, the C/P of exported OM was estimated using the empirical relationship between C/P of particles and surface PO_4 concentrations (Tanioka & Matsumoto, 2017). This approach yielded a range in C/P from ~70 to 270 with a mean global C/P of 135 (50°S to 50°N), which is significantly greater than the Redfield ratio of 106 (Redfield, 1958) but similar to the global mean C/P of 146 observed for suspended particles (Martiny et al., 2013). Errors in the fraction of export supported by surface advective PO_4 and DOP flux account for errors in the nutrient flux and observed export.

3. Results

3.1. OM Export in the Pacific Ocean

O_2 budget-based estimates of OM export for the Pacific Ocean range with latitudes from 0.5 to 3 mols C/m²/yr and yield a basin-wide (50°S to 50°N) mean rate of 2.4 ± 0.9 mol C/m²/yr (Table 1, Figure 3). Uncertainty

Table 1
Estimates of Mean (±1 SD) Organic Matter Export Rate (mol C/m^2/yr) at the Winter Mixed Layer Depth Based on Surface O_2 and DIC + DIC^{13} Budgets (This Work) and Current and Prior Estimates Based on O_2, O_2/Ar, DIC, NO_3 and PO_4 Budgets and Oxygen Utilization Rates Between 50°S and 50°N (See Text and Figure 3)

Ocean basin	OM export (O_2 budget)	OM export (DIC^{13} budget)	OM export (all estimates)	Number of observations	Export fraction supplied by surface nutrients
N. Pacific	2.7 ± 0.6	2.0 ± 0.5	2.5 ± 0.7	39	0.49 ± 0.19
S. Pacific	1.9 ± 1.0	1.3 ± 0.4	1.9 ± 0.8	23	0.48 ± 0.27
Pacific	2.4 ± 0.9	1.6 ± 0.6	2.1 ± 0.8	62	0.48 ± 0.23
N. Atlantic	3.5 ± 1.0	2.1 ± 0.7	2.8 ± 0.9	34	0.20 ± 0.16
S. Atlantic	2.2 ± 1.0	2.4 ± 0.7	2.3 ± 0.9	20	0.14 ± 0.15
Atlantic	2.8 ± 1.2	2.2 ± 0.8	2.6 ± 0.9	54	0.17 ± 0.16
S. Indian	0.7 ± 1.3	0.4 ± 0.1	0.9 ± 0.8	18	0.20 ± 0.26
Global Ocean	2.2 ± 1.0	1.5 ± 0.5	2.0 ± 0.8	134	0.35 ± 0.22

Note. Final column lists fraction of observed export that is supported by PO_4 and DOP transport via surface advection (see text).

in mean values represent ±1 SD of estimates unless otherwise specified. DIC^{13} budget-based estimates of OM export range from 1 to 3 mol C/m^2/yr with a basin-wide mean of 1.6 ± 0.6 mol C/m^2/yr. The PO_4 based estimate of OM export in the equatorial Pacific was 2.9 ± 0.9 mol C/m^2/yr. Previous budget-based estimates of OM export include mean rates of 2.6 ± 0.7 mol C/m^2/yr at Sta ALOHA (23°N 158°W) and 3.3 ± 1.8 mol C/m^2/yr for the equatorial Pacific (Emerson, 2014), 1.8 ± 0.6 at OSP (50°N, 145°W) (Emerson, 2014; Fassbender et al., 2016; Haskell et al., 2020), 1.6 ± 1.1mol C/m^2/yr for subpolar N. Pacific (Palevsky et al., 2016), 1.8 ± 0.3 and 0.6 ± 0.4 mol C/m^2/yr for subtropical N. and S. Pacific (Yang et al., 2017), respectively (Figure 3). OUR-based estimates of OM export are 1.2 ± 1.1 mol C/m^2/yr for the Southern Ocean (Arteaga et al., 2019), 2.2 ± 0.4 mol C/m^2/yr for the S. Pacific (60°S–30°S) (Sonnerup et al., 2015) and 2.6 ± 0.8 mol C/m^2/yr for the N. Pacific (25°N– 47°N) (Sonnerup et al., 1999) (Figure 3). Meridional patterns in OM export based on all estimates show the lowest rates in the subtropical S. Pacific at 1.5 ± 0.8 mol C/m^2/yr and higher rates of 2.9 ± 0.9 mol C/m^2/yr at the equator and in the N. Pacific at 2.5 ± 0.7 mol C/m^2/d ($P > 0.1$). The basin-wide (50°S–50°N) mean OM export is 2.1 ± 0.8 mol C/m^2/yr based on the compilation of OM export rate estimates in this study and previously (Table 1).

3.2. OM Export in the Atlantic Ocean

O_2 budget-based estimates of OM export for the Atlantic Ocean range from 1 to 5 mols C/m^2/yr and yield a basin-wide (with latitudes from 50°S to 50°N) mean rate of 2.8 ± 1.2 mol C/m^2/yr (Table 1, Figure 3). DIC + DIC^{13} budget-based estimates of OM export range from 1 to 4 mol C/m^2/yr with a basin-wide mean of 2.2 ± 0.8 mol C/m^2/yr. The PO_4 based estimate of OM export in the equatorial Atlantic was 2.0 ± 1.0 mol C/m^2/yr. Previous budget-based estimates of OM export (O_2, DIC, NO_3) rates of 3.0 ± 1.0 mol C/m^2/yr at BATS (32°N 64°W) (Fawcett et al., 2018), 3.4 ± 0.5 at ESTOC (29°N, 15°W) (Neuer et al., 2007), 2.6 ± 2.5 mol C/m^2/yr (Ostle et al., 2015) and 3.0 ± 0.5 mol C/m^2/yr (Quay et al., 2020) for subtropical and subpolar N. Atlantic, 1.2 ± 0.4 mol C/m^2/yr (Yang et al., 2019) and 2.9 mol C/m^2/yr (Billheimer et al., 2021) for subtropical N. Atlantic. OUR-based estimates of OM export are 1.0 ± 0.9 mol C/m^2/yr for the Southern Ocean (70°S to 50°S) and 2.7 ± 0.8 mol C/m^2/yr for the subpolar (50°S to 35°S) S. Atlantic (Arteaga et al., 2019). OM export in the N. Atlantic (2.8 ± 0.9 mol C/m^2/yr) is slightly higher ($P > 0.1$) than in the S. Atlantic (2.3 ± 0.9 mol C/m^2/yr). The basin-wide (50°S–50°N) mean OM export is 2.6 ± 0.9 mol C/m^2/yr based on new and previous estimates (Table 1).

3.3. OM Export in the S. Indian Ocean

O_2 budget-based estimates of OM export range from −1 to 3 mols C/m^2/yr and yield a basin-wide (with latitudes 50°S to 0°N) mean rate of 0.7 ± 1.3 mol C/m^2/yr (Table 1, Figure 3). DIC^{13} budget-based estimates of OM export
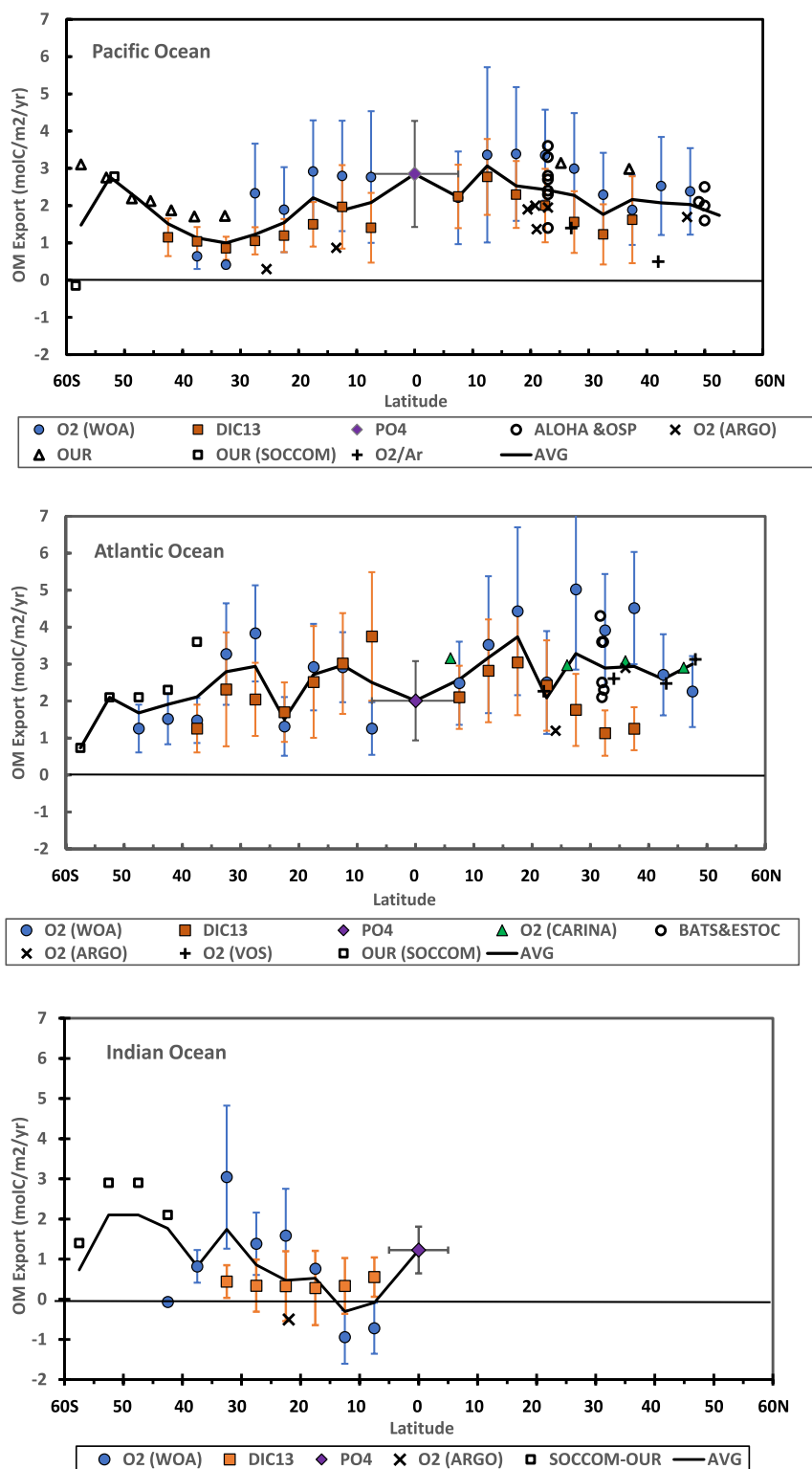
Figure 3. Meridional pattern in annual organic matter export for Pacific, Atlantic and Indian oceans based on O_2 (blue filled circles), DIC + DIC13 (red filled squares) and PO_4 (diamond) surface budgets (this work) and previous estimates based on annual O_2 budgets from ARGO floats, container ship measurements and CARINA climatological data, O_2/Ar budgets, oxygen utilization rates (OUR) and at time series sites ALOHA, Ocean Station Papa and ESTOC (see text). The annual export rate averaged basin-wide and over 5° latitude bands based on all estimates (solid line). Error bars ($\pm$1 SD) included for export estimates determined from O_2 and DIC + DIC^{13} and PO_4 budgets (this work).

range from 0.3 to 0.6 mol C/m^2/yr with a basin-wide mean of 0.4 ± 0.1 mol C/m^2/yr. The O_2 and DIC^{13} based estimates exclude the region north of the equator because of the high seasonal variability of biological productivity and circulation caused by monsoons. The PO_4 based estimate of OM export in the equatorial Indian Ocean was 1.2 ± 0.5 mol C/m^2/yr. Previous O_2 budget-based estimates of OM export yielded a rate of −0.5 ± 0.5 mol C/m^2/yr in the eastern subtropical S Indian (Yang et al., 2019). OUR-based estimates of OM export yielded rates of 1.7 ± 1.1 mol C/m^{2}yr in S. Ocean (62°S–50°S) and 2.5 ± 0.6 mol C/m^2/yr in the subpolar S. Indian (Arteaga et al., 2019). The basin-wide (50°S–0°) mean OM export rate is 0.9 ± 0.8 mol C/m^2/yr based on new and previous estimates (Table 1).

4. Discussion

4.1. Budget-Based OM Export for All Ocean Basins

Overall, there is about a factor three range in the OM export rates, that is, >75% of the estimates are between 1 and 3 mols C/m2/yr (Figure 3). Regionally, the lowest export rates (1–1.5 mol C/m2/yr) are found in the subtropical gyres of the S. Pacific and S. Indian oceans and the highest rates (2.8 ± 1.0 mol C/m^2/yr) are found in the N. Atlantic. In both the Atlantic and Pacific oceans, the mean export rate in the northern basin is 20%–30% higher than in the southern basin ($P > 0.1$). The mean OM export in the S. Indian Ocean (0.9 ± 0.8 mol C/m^2/yr) is about half the export in the S. Atlantic and S. Pacific oceans at 2.3 ± 0.8 and 1.9 ± 0.8 mol C/m^2/yr, respectively. Lower export rates in the S. Indian are unexpected as ocean ecosystem models typically yield similar export rates for all three basins (e.g., Laufkötter et al., 2016; Letscher et al., 2016). The low mean OM export rate for the Indian Ocean does not appear to be biased because of the lack of data as the number of O_2 saturation observations (WOA) for the S. Indian are within 5% of the observations for the S. Atlantic and S. Pacific and the number of δ^{13}C-DIC surface measurements and depth profiles in the S. Indian exceeds that in the S. Atlantic (GLODAP). Furthermore, the overall number of OM export estimates for the S. Indian ($n = 18$) is similar to that for the S. Atlantic ($n = 20$) and S. Pacific ($n = 23$) oceans and low export rates are estimated by both the O_2 and DIC + DIC^{13} budgets (Table 1). Thus, the data in hand indicate that OM export rates are lower in the S. Indian compared to S. Pacific and S. Atlantic ($P < 0.1$).

The area weighted global OM export rate is 2.0 ± 0.8 mol C/m^2/yr at the depth of the winter mixed layer, which corresponds to 8.6 ± 3.5 Pg C/yr. Our observation based global OM export rate is in line with OM export predicted by ocean models that determine the OM export flux (typically at base of photic layer) based on the constraint of matching observed dissolved nutrient distribution in upper ocean which yield a range of ∼9–12 Pg C/yr (e.g., Bopp et al., 2001; Najjar et al., 2007; Schlitzer, 2002) and models that rely on satellite-based PP coupled with empirically determined e-ratios which yield a range of 8–11 Pg C/yr (e.g., Dunne et al., 2007; Laws et al., 2011; Li & Cassar, 2016). In contrast, our observation-based OM export rate is almost twice the OM export rate of 4–6 Pg C/yr estimated by ecosystem models that are tuned to yield observed particle sinking fluxes at the photic layer depth yield (e.g., Bisson et al., 2018; Siegel et al., 2014). Regionally, the subtropical gyres account for ∼45% of the estimated global export with the equatorial region making the highest contribution in the Pacific (∼45%) and the subpolar region being highest (∼45%) in the S. Indian oceans.

4.2. Pathways Supplying Dissolved Nutrients Supporting OM Export

The estimates of OM export for the three major ocean basins presented above provide an opportunity to investigate the pathways and processes supplying the dissolved nutrients that support export. Here, the focus is on the supply of PO_4 and dissolved organic phosphate (DOP), rather than NO_3, to avoid the complications resulting from N fixation. There are consistent meridional patterns in surface nutrients (PO_4) with the highest concentrations in the Southern Ocean and lowest concentrations in the subtropical gyres, maxima in northern subpolar latitudes that are much higher in the Pacific than Atlantic and a maximum in the equatorial Pacific that is not observed in the equatorial Atlantic or Indian basins. It is worth noting that the regions where there are significant surface PO_4 concentrations are the same regions where there are negative surface O_2 saturation levels during all or part of the year (Figure 1; Figure S2 in Supporting Information S1). Regions with high surface PO_4 concentrations and negative O_2 supersaturation levels occur when the supply rate of subsurface waters with high nutrient and low O_2 concentrations exceeds the OM export rate. Surface DOP has a much smaller meridional range (0.1–0.3 μM) than PO_4 (<0.05 to >1.5 μM) with maximum concentrations occurring in the equatorial Pacific (Figure 4). A
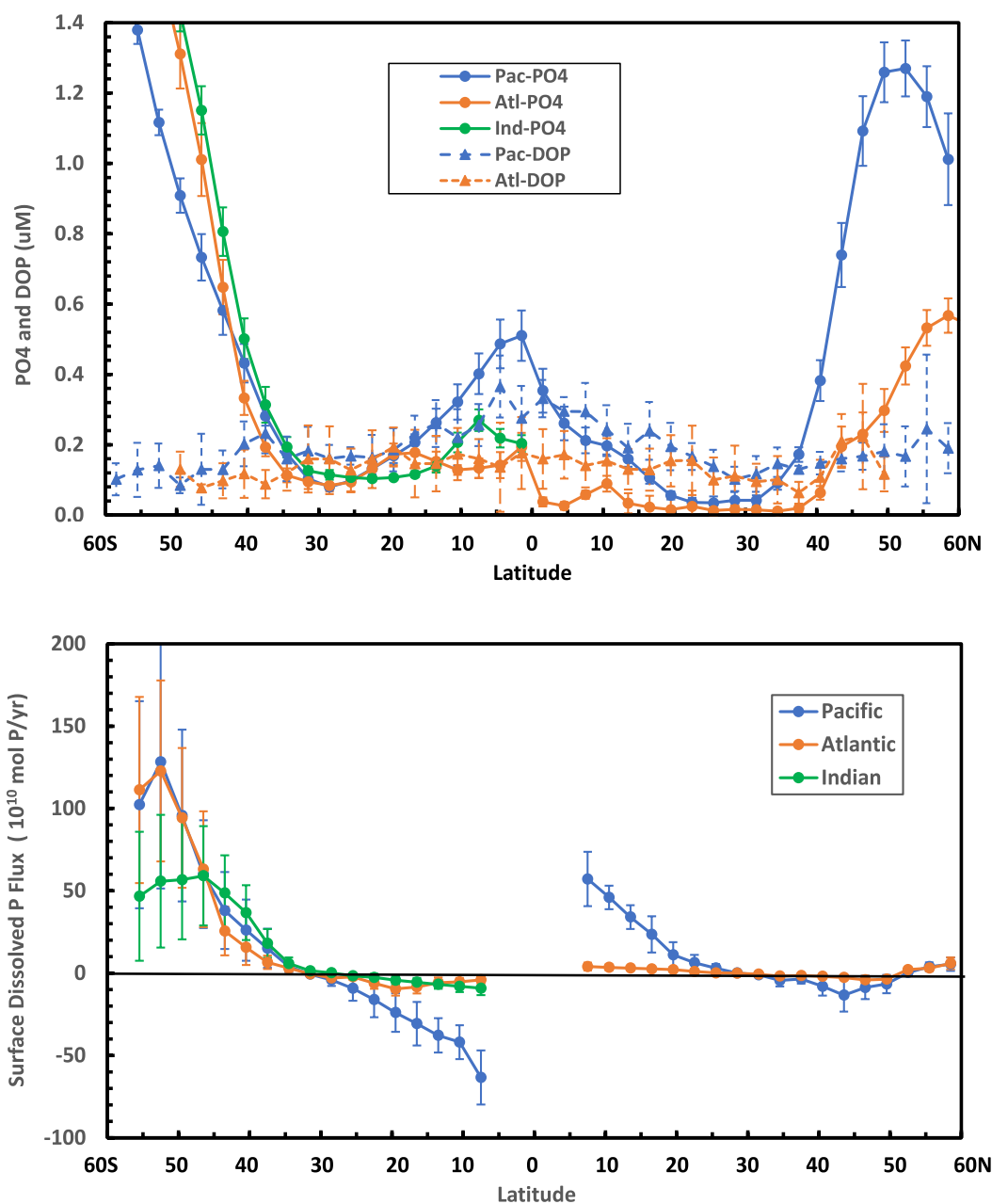
Figure 4. Latitudinal pattern in surface PO$_4$ and DOP concentrations (top) and meridional surface advective PO$_4$ and DOP flux (bottom, with + = northward) integrated zonally across each basin and averaged over 3° latitude bands. Error bars represent ±1SD in zonal means. For Indian ocean, only PO$_4$ transport is calculated because of the lack of DOP data.

maximum in northward surface PO$_4$ and DOP transport occurs ∼50°S in all basins and then decreases to near zero by 30°S (Figure 4). High rates of poleward surface PO$_4$ and DOP transport occur in the equatorial Pacific but not in the equatorial Atlantic nor Indian basins, with the primary reason being the difference in surface PO$_4$ and DOP concentrations (Figure 4).

Dissolved nutrients can be supplied to the photic layer either from below via turbulent mixing, eddy pumping and upwelling or horizontally via surface advection and eddy transport. It isn't clear which supply processes dominate especially in the subtropical gyres where surface nutrient concentrations approach zero and the nutracline is often deeper than the base of the photic layer. The abundance of PO$_4$ in the surface layer of the Southern Ocean, subpolar N. Atlantic and N. Pacific basins, and the equatorial Pacific identify these regions as potentially important nutrient sources (Figure 4).

The estimates of surface dissolved PO_4 and DOP flux and the budget-based estimates of OM export rates on global scales presented here allow one to identify likely sources and pathways of nutrient supply fueling global OM export and the relative importance of vertical versus horizontal processes supplying nutrients. The mechanisms supplying nutrients to the photic layer, especially in the subtropical gyres, have been debated for decades (e.g., Billheimer et al., 2021; Jenkins & Doney, 2003; McGillicuddy et al., 2007; Williams & Follows, 1998). Most of the insight gained into pathways of nutrient supply rely on the output from ocean models where the dissolved nutrient transport and OM export rates can be inventoried. Here, the importance of nutrient source regions is determined based on observed surface velocities, dissolved PO_4 and DOP distributions (Figure 4) and OM export rates (Figure 3), which can be compared to model findings.

4.2.1. Southern Ocean Nutrient Source

A notable model-based conclusion underscored the importance of the Southern Ocean as a major nutrient source supporting global OM export (Sarmiento et al., 2004). By comparing OM export for two model scenarios, one with observed PO_4 and one with zero PO_4 in the surface layer of the Southern Ocean, Sarmiento et al. concluded that $\sim$75% of the global OM export relied on nutrients that originated in the Southern Ocean. More recently, using a data assimilation model, Primeau et al. (2013) found that the complete consumption of nutrients in the Southern Ocean yielded a 44% decrease in OM export north of 40°S. This same issue is addressed here using observations. The northward surface transport of PO_4 and DOP at 50°S integrated zonally across all ocean basins including the transport from advection based on drifter velocities and eddy mixing was determined, as discussed above (Figure 4).

The northward transport of dissolved PO_4 and DOP in the surface layer at 50°S in all basins potentially supports an average global OM export rate of 1.4 ± 0.6 mol C/m^2/yr assuming this PO_4 and DOP transport is offset by OM export spread evenly across the global ocean north of 50°S with a C/P of 135 based on the C/P predicted from surface PO_4 concentration, as discussed above. In comparison, budget-based estimates of OM export north of 50°S presented here yield a global mean of 2.0 ± 0.8 mol C/m^2/yr which implies that surface nutrients in the Southern Ocean transported northward could potentially fuel $\sim$70 $\pm$ 38% of the global export, where the uncertainty represents errors ($\pm$1 SD) in the dissolved P flux and export estimates. Thus, previous model output and current observations indicate that the Southern Ocean is a primary source of nutrients supporting OM export globally.

It is important to realize that the mechanism delivering nutrients which originated in the Southern Ocean to the photic layer throughout most of the ocean (north of 30°S) must depend on vertical processes (e.g., upwelling, turbulent mixing, eddy pumping, etc) because the northward surface advective transport of PO_4 and DOP reaches zero by 30°S (Figure 4). The sharp decrease in equatorward surface velocity (water transport) and advective PO_4 and DOP flux between 50°S and 30°S is a result of subpolar surface waters subducting below the warmer and less dense surface waters of the subtropical gyre. This subduction is related to formation of SubAntarctic Mode Water (SAMW) with a density range of 26.5–27.1 and SubTropical Mode Water (STMW) with a density range of $\sim$26–26.5 (e.g., Sarmiento et al., 2004; Tsuchiya & Talley, 1998). The subducting STMW and SAMW water masses spread northward at depth and eventually reach the equatorial region where they contribute to the Equatorial Undercurrent (Goodman et al., 2005). A relevant observation is that the mean depth of the 26.5 isopycnal is significantly deeper in the Pacific than in the Atlantic and Indian oceans (Figure 5). Northward of 30°S in the Pacific, the depth of the 26.5 isopycnal ranges from 200 to 500 m, which lies significantly below the photic layer, whereas in the Atlantic, the depth of the 26.5 isopycnal ranges is shallower ranging from 100 to 300 m and is within reach of the photic layer. Furthermore, the stability of the upper 500 m of the water column (expressed as the Brunt-Vaisala frequency) is significantly lower in the Atlantic than in the Pacific basin (Figure 5). The density distribution in the Indian Ocean is intermediate between the extremes of the Pacific and Atlantic oceans. Thus, the combination of shallower isopycnal depths and lower water column stability, which enhances turbulent mixing (Osborn, 1980) suggests that preformed nutrients originating in the surface water of the Southern Ocean and subducted northward via STMW and SAMW are more likely to be supplied vertically to the photic layer in the Atlantic Ocean than in the Pacific basin. Estimates of surface meridional advective dissolved P supply rates support the importance of vertical nutrient supply in the Atlantic Ocean, as discussed below.

4.2.2. Equatorial Ocean as a Nutrient Source

A notable observation is that the surface PO_4 concentration in the equatorial Pacific is 2–3 fold higher than that in the equatorial Atlantic and Indian oceans (Figure 4). This observation could in part be related to the depth of the 26.5 isopycnal (STMW) in the Pacific north of 30°S which is within reach of the base of the photic layer
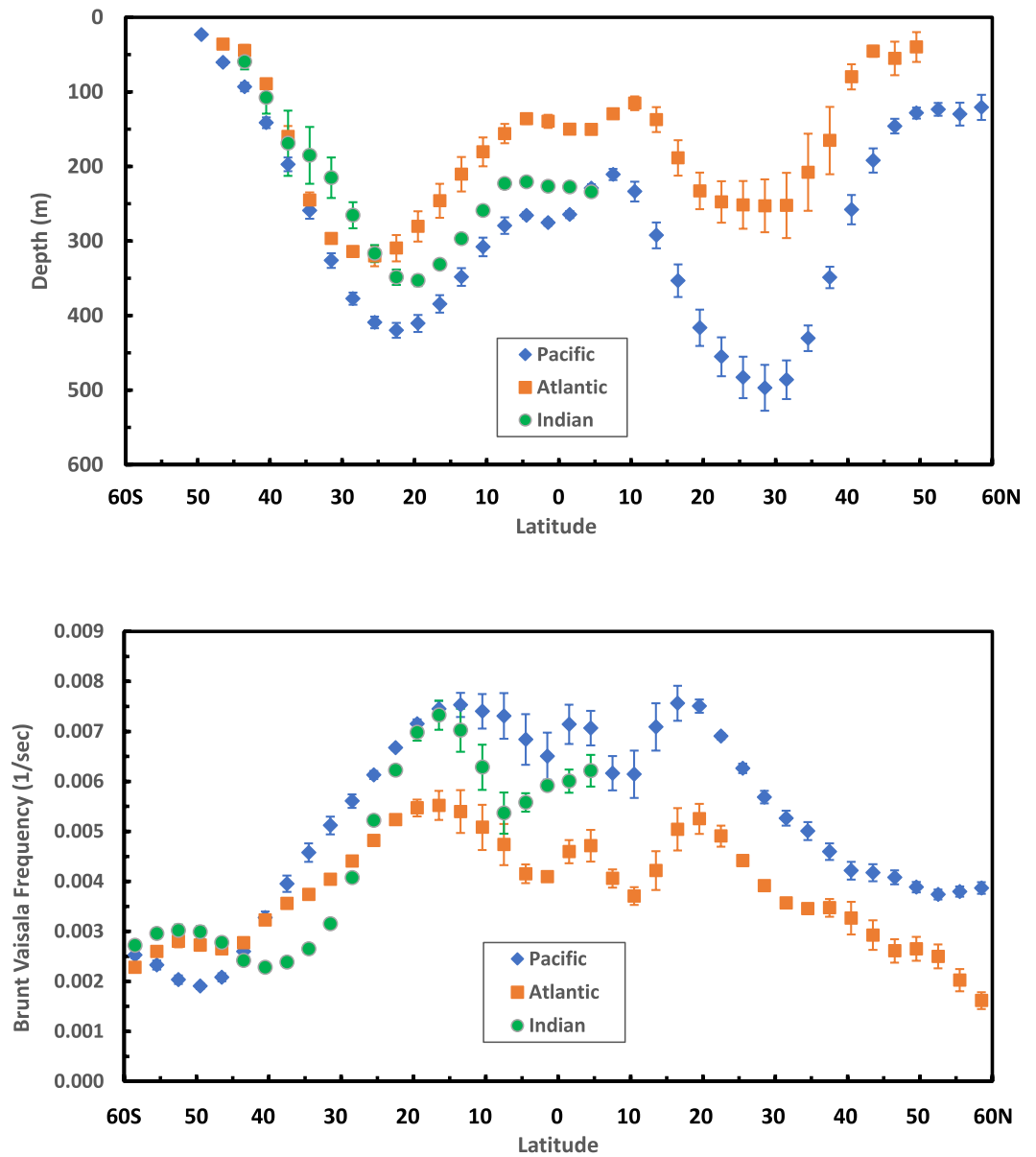
Figure 5. The meridional pattern in the depth of the $\sigma_\Theta = 26.5$ isopycnal (top) and Brunt-Vaisala frequency between the base of the mixed layer and 500 m (bottom) averaged zonally across each basin and by 3° latitude bands. Error bars represent ± 1SD in zonal means.

(∼200 m) only in the equatorial region (Figure 5) and implies that preformed nutrients on this isopycnal originating in the Southern Ocean are unlikely to be consumed by biological productivity until they reach the equatorial region. In contrast, the depth of the 26.5 isopycnal in the Atlantic is ∼100 m shallower and water column stability is weaker than in the Pacific; thus, preformed nutrients on this isopycnal originating in the Southern Ocean are more likely to be consumed by biological productivity before they reach the equatorial region. Additionally, the surface PO_4 concentration at the northern outcrop of the 26.5 isopycnal (∼50°N) is significantly higher in the Pacific at 1.3 μmol kg^{-1} than in the Atlantic at 0.3 μmol kg^{-1} (Figure 4), which would increase nutrient concentrations on this isopycnal in the equatorial Pacific. The result is that the water upwelling in the Pacific has a PO_4 concentration (∼0.6 μmol kg^{-1}) significantly higher than that in the Atlantic (0.4 μmol kg^{-1}) at the maximum annual mixed layer depth (∼60–70 m), which also corresponds to the depth of maximum upwelling velocity at the equator (Johnson et al., 2001). Additionally, stronger iron limitations on biological productivity would potentially yield higher surface PO_4 concentrations in the equatorial Pacific versus Atlantic basins. Thus, as a result of

nutrient supply and biological uptake limitations, there is a significant excess of dissolved nutrients in the surface layer of the equatorial Pacific Ocean that is not observed in the Atlantic or Indian basins (Figure 4).

High surface PO_4 concentration in the equatorial Pacific implies that the poleward Ekman divergence in the surface layer is a source of PO_4 supply to the subtropical gyres in the N. and S. Pacific. Similarly, surface DOP concentrations in the equatorial Pacific at ∼0.3 µmol kg⁻¹ are significant compared to PO_4 concentrations at ∼0.5 µmol kg⁻¹ and are an additional potential dissolved nutrient source for the subtropical gyres. The poleward advective and eddy flux of surface PO_4 and DOP were determined at 8°N and 8°S based on drifter velocities, as discussed above, with the 8° latitude boundary being chosen to avoid the impact of downwelling and equatorial convergence of surface waters that occurs nearer the equator (Johnson et al., 2001). In summary, dividing the surface advective and eddy fluxes of PO_4 and DOP by the surface areas of the N. and S. Pacific (8°–50°) and multiplying by a C/P of 125 yielded an estimated OM export rate of 0.8 ± 0.2 mol C/m^2/yr potentially supported by equatorial surface nutrient delivery which is ∼37 ± 14% of the observed OM export in the basin. In contrast, the poleward surface PO_4 and DOP flux in the equatorial Atlantic would support only ∼5% of the observed OM export. The situation in the S. Indian Ocean lies between these extremes with southward equatorial surface PO_4 at 8°S supporting ∼15% of the observed OM export. (Note that the Indonesian Throughflow is another potential nutrient source to the Indian Ocean based on Ayers et al., 2014).

4.2.3. Processes Supplying Nutrients to the Subtropical Gyres

The mechanisms supplying nutrients to the subtropical gyres have been debated for quite a while with the major conundrums being the low dissolved nutrient concentrations in the surface layer which yield low rates of horizontal nutrient supply, the separation between the depths of the photic layer and nutracline, and the portion of OM export supported by DOP. Several studies highlight the role of western boundary currents. Jenkins and Doney (2003) described a "nutrient spiral" which involved an upward flux of nutrients by enhanced vertical mixing occurring along the path of the Gulf Stream with these nutrients being distributed throughout the gyre by isopycnal mixing and brought into the photic layer by local vertical processes (convection, eddy heaving, turbulence, etc). Williams et al. (2006) used model output to demonstrate the importance of the Gulf Stream as a nutrient stream which delivers nutrients deeper in the water column to the surface layer of the subpolar ocean, which can then be transported southward into the subtropical gyre. Recently, Liao et al. (2022) found evidence for enhanced upwelling associated with western boundary currents that can deliver nutrients from depth into the photic layer. Several studies have focused on the role of eddies. McGillicuddy et al. (2007) demonstrated that eddies can increase biological productivity through enhanced upwelling of nutrients in the subtropical N. Atlantic. Johnson et al. (2010) found that eddy events (∼monthly) in the subtropical N. Pacific were a major source of nutrient input into the photic layer from below through isopycnal heaving. Models have demonstrated that eddies and submesoscale processes can enhance the horizontal and vertical transport of nutrients at the subpolar-subtropical front (e.g., Mahadevan, 2016; Oschlies & Garcon, 1998).

Several studies have focused on the role of DOP as a dissolved nutrient source in the subtropical gyres with most insights based on modeling results. Letscher et al. (2016) used an ecosystem model to conclude that 22%–46% of OM export in the five subtropical gyres was supported by horizontal DOP transport. Reynolds et al. (2014) used an eddy resolving model to conclude that 70% of the particle export in the subtropical N. Atlantic was supported by DOP supply. A key assumption in these model experiments is the proportion of total DOP supplied that is sufficiently labile (semi-labile) to be degraded and used to fuel primary production by plankton, for example, Reynolds et al. assumes 95% of DOP is semi-labile. There are only a few observation-based estimates of the importance of DOP as a dissolved P source in the subtropical gyres. For example, Abell et al. (2000) and Mahaffey et al. (2004) relied on observed horizontal gradients of surface DOP and PO_4 and estimates of advection rates to determine transport of DOP and PO_4 and found that the poleward surface flux of DOP from the equatorial to subtropical regions exceeded the PO_4 flux in the N. Pacific and Atlantic oceans. Mather et al. (2008) used measurements of DOP and alkaline phosphatase to conclude that the turnover time of surface DOP differed by ∼20-fold between 0.5 and 10 years for the subtropical N. and S. Atlantic, respectively, and estimated that DOP utilization could support between 20% and 5% of the primary production rates in these two subtropical systems.

A plot of surface DOP versus PO_4 (Figure 6) concentrations (Knapp et al., 2021; Martiny et al., 2019) along a meridional section between 30°S and 30°N and a zonal section between the eastern and western boundaries of the subtropical gyre (averaged zonally in 10° bins and meridionally in 5° bins) for the Atlantic and Pacific oceans yields a slope of ∼0.47 ± 0.10 and intercept of ∼0.13 ± 0.01 which has two significant implications. The
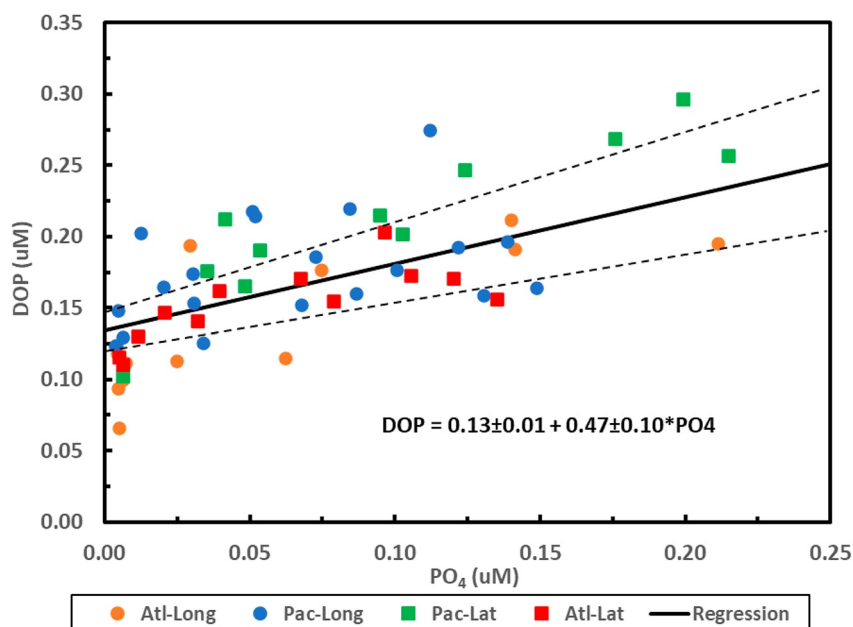
Figure 6. The surface concentrations of dissolved DOP (Knapp et al., 2021) and PO$_4$ (Martiny et al., 2019) for the subtropical Atlantic and Pacific Oceans averaged zonally (10° longitude bins) across each basin between 15° and 30° (-Long) and meridionally (5° latitude bins) between 30°S and 30°N (-Lat) in each basin. The linear regression relationship and uncertainty are shown. PO$_4$ data supplemented with GLODAP data (Lauvset et al., 2016) corrected for offset from PO$_4$ data set of Martiny et al. (2019) when PO$_4$ < 0.10 μM.

slope implies that, on average, the meridional and zonal transport of surface PO$_4$ into the subtropical gyres is about twice that for DOP. Thus, on average, two-thirds of dissolved P supplied by surface advection and mixing is from PO$_4$ and one-third from DOP. Assuming that the intercept represents the average concentration of the surface DOP pool that is unused within the subtropical gyres, it represents about 40% of the DOP concentration (~0.3 μM) supplied from the edges of the subtropical gyres, which is substantially greater than the 5% assumed in some model simulations and, in turn, reduces the impact of DOP on fuel export in the gyres.

The importance of horizontal surface nutrient supply to the subtropical gyres (15°–35°) was addressed by comparing the calculated meridional and zonal advective transport of PO$_4$ and DOP in the surface layer, discussed above, to the observed OM export rate. The net advective flux of PO$_4$ and DOP accounts for the portion of PO$_4$ and DOP that remains unconsumed in the gyre (i.e., 0.01–0.1 μmol kg^{-1} for PO$_4$ and ~0.1 μM for DOP). A steady-state balance between the dissolved P supply and organic P export is assumed. The estimated organic P export is multiplied by the C/P of exported OM to compare to the O$_2$ and DIC[13] budget-based estimates of OM export (mol C/m^2/yr). This brings up an important point, that is, the C/P of exported OM in the subtropics is much higher than the Redfield ratio of 106. Martiny et al.'s (2013) compilation of the elemental ratio for suspended particles yielded C/P values from 171 to 226 for the subtropical gyres in the N. Pacific and N. Atlantic oceans. The importance of DOM export in the subtropics has been increasingly recognized (e.g., Fawcett et al., 2018) with the labile DOM likely having a C/P > 200 (e.g., Hopkinson & Vallino, 2005). Here, the C/P of export was estimated from the surface PO$_4$ concentrations, as discussed above, and yielded values of ~140 for the subtropical gyres in the S. Pacific, S. Indian and S. Atlantic and 185 and 250 for the subtropical gyres in the N. Pacific and N. Atlantic, respectively, which agreed with observations by Martiny et al. (2013).

The surface meridional and zonal advective fluxes of PO$_4$ and DOP into the subtropical gyres (15°–35°) yield a dissolved P surface flux of 9.4, 7.4, and 4.3 mmol P/m^2/yr into the subtropical gyres in the S. Pacific, S. Atlantic and S. Indian oceans, respectively, which would support OM export rates of 1.3, 1.0, and 0.6 mol C/m^2/yr. (The surface DOP flux in the Indian Ocean is assumed to be 47% of the PO$_4$ flux based on slope in Figure 6 because of lack of DOP data). In the N. Pacific and N. Atlantic, the surface advective dissolved PO$_4$ and DOP fluxes supply 6.9 and 3.6 mmol P/m^2/yr to the subtropical gyres, respectively, which would support OM export rates of 1.3 and 0.9 mol C/m^2/yr. Mahaffey et al. (2004) estimated a meridional surface DOP flux to the subtropical S. Atlantic based on DOP measurements and advection rates that would support an OM export of 0.7 mol C/m^2/yr (assuming

C/P = 140) which agrees with the estimate presented here. The observed OM export rates were 1.5 ± 0.4, 2.5 ± 0.4, and 0.9 ± 0.5 mol C/m^2/yr for the subtropical S. Pacific, S. Atlantic, and S. Indian oceans, respectively, which implies that horizontal surface PO$_4$ and DOP supply could potentially support $\sim 89 \pm 48\%$, $41 \pm 16\%$, and $70 \pm 64\%$ of the observed OM export, respectively. In the subtropical N. Pacific and N. Atlantic the observed OM export rates were 2.3 ± 0.4 and 3.0 ± 0.6 mol C/m^2/yr, respectively, and imply that the horizontal supply of surface nutrients could fuel $\sim 57 \pm 22\%$ and $30 \pm 14\%$ of the export in these subtropical gyres. These results suggest that horizontal supply of surface PO$_4$ and DOP is the dominant nutrient source for the subtropical Pacific, mainly because of the poleward transport of surface nutrients from the equatorial region, whereas vertical supply of nutrients dominates in the subtropical N. Atlantic likely because of the weak equatorial source and enhanced nutrient supply via vertical mixing, eddy activity and upwelling associated with the Gulf Stream (e.g., Jenkins & Doney, 2003; Liao et al., 2022; McGillicuddy et al., 2007; Williams et al., 2006).

The model-based results of Letscher et al. (2016) indicate that horizontal supply of PO$_4$ and DOP support 44%–67% of the export in the subtropical gyres of the Pacific, Atlantic and Indian oceans, whereas the observation-based estimates of the fraction of horizontal dissolved PO$_4$ and DOP supply presented here vary from 30% to 90%. The model used by Letscher et al. indicates that total organic P exported from the subtropical gyres of all basins varies by $\sim 50\%$ (8–12 mmol P/m^2/yr) whereas our observed OM export in the gyres varies by $\sim 2\times$ (4–9 mmol P/m^2/yr using C/P estimated from PO$_4$). Overall, the observations show more inter-basin variability in export rate and mechanism of supply for subtropical gyres compared to the model results.

4.2.4. Role of Nutrient Limitation on Export

Nutrient (N, Fe, Si) limitation plays an important role in the regional pattern of OM export. In the HNLC regions, Fe (and in some regions Si) availability limits primary production especially by diatoms and thus lowers export, whereas in the subtropical gyres, Fe limitation reduces N fixation rates that prevent the complete utilization of dissolved P (e.g., Boyd et al., 2007; Martiny et al., 2019; Mills et al., 2004). If Fe supply to the surface layer of the Southern Ocean were increased and caused an increase in OM export, then a consequence would be a decrease in surface nutrient concentrations, which in turn would cause reduced OM export to regions outside the Southern Ocean, as the model experiments of Sarmiento et al. (2004) and Primeau et al. (2013) demonstrated. A similar situation would exist in the equatorial Pacific Ocean where an increased supply of Fe would increase OM export locally but decrease the poleward supply of surface nutrients to the adjacent subtropical gyres. Thus, reducing Fe limitations from the levels existing in today's ocean would likely increase regional variations in export, that is, higher rates in HNLC regions and lower rates in subtropical gyres, but the impact on global export would likely be significantly less as some of the regional variations would be offset. That is, the global export balances the rate of PO$_4$ supplied to the photic layer by upwelling and vertical mixing minus the loss of unused PO$_4$ downwelling within the subtropical gyres.

Currently, there is unused dissolved PO$_4$ in the surface layer of the subtropical gyres with significantly higher concentrations in the S. Pacific and S. Atlantic and S. Indian basins (~ 0.06–0.10 µmol kg^{-1}) than in the N. Pacific and N. Atlantic (<0.02 µmol kg^{-1}) as observed previously by Martiny et al., 2019 (Figure S4 in Supporting Information S1). If the supply of the limiting nutrient(s) to all the subtropical gyres was increased to utilize all the remaining PO$_4$ in the gyres, this would yield a <0.1 mol C/m^2/yr increase in export in the subtropical N. Pacific and N. Atlantic, a 0.3 ± 0.1 mol C/m^2/yr increase in the subtropical S. Pacific and S. Atlantic and a 0.8 ± 0.2 mol C/m^2/yr increase in the subtropical S. Indian ocean, which in turn, would yield a 0.4 ± 0.1 Gt C/yr increase in export globally. Thus, current limitations on P utilization appear to have a greater effect in limiting OM export in the southern versus northern subtropical gyres and, particularly, in the S. Indian Ocean.

5. Conclusions: Inter-Basin Variations of OM Export and Nutrient Supply

Budget-based OM export rates for the Atlantic and Pacific oceans are similar at 2.1 ± 0.8 to 2.6 ± 0.9 mol C/m^2/yr and about twice that observed for the S. Indian at 0.9 ± 0.8 mol C/m^2/yr (Table 1). Despite similar export rates, the pathways of nutrient supply differ markedly between the Atlantic and Pacific basins (Figure 7). Although the Southern Ocean is potentially a dominant source of dissolved nutrients supporting $70 \pm 38\%$ of OM export globally, the northward transport of surface nutrients is nearly zero at $\sim 30°$S in all basins (Figure 7). Thus, preformed nutrients originating in the Southern Ocean that support OM export must be delivered by vertical processes (upwelling, turbulent mixing, eddy pumping) to most of the ocean. In the Pacific, equatorial upwelling is an important pathway of nutrient supply but not in the Atlantic (or Indian) basin (Figure 7). North of 30°S the combined surface horizontal transport of PO$_4$ and DOP in the equatorial region (poleward) and at 50°N (southward) support $48 \pm 23\%$
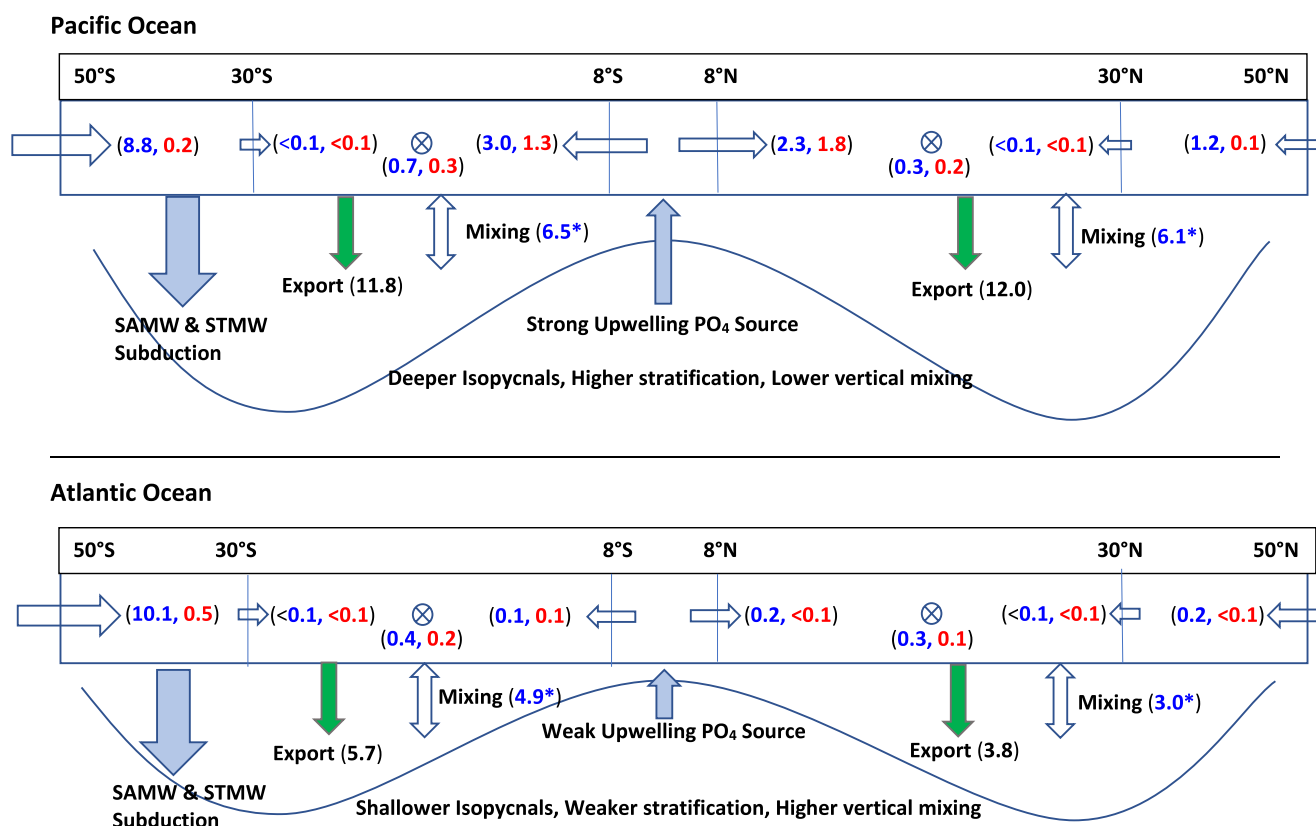
Figure 7. PO_4 (blue) and DOP (red) fluxes (10^{11} mols P/yr) estimated from meridional (arrows) and zonal ($\otimes$) surface currents and observed organic matter export and supplied by vertical mixing in the Pacific and Atlantic oceans where the vertical mixing flux is calculated (*) assuming a steady-state balance between total P supply and export. Characteristics in the isopycnal depth, water column stratification, vertical mixing, and equatorial upwelling (<500 m), which impact the pathway of PO_4 and DOP supply for the Pacific and Atlantic oceans are shown. Subduction of Subantarctic Mode Water (SAMW) and Subtropical Mode Water (STMW) on surface water and P transport is shown. See text for discussion.

of the observed OM export in the Pacific but only $17 \pm 16\%$ in the Atlantic basin. Two factors that may impact the dominance of vertical nutrient supply in the Atlantic basin are the shallower depth of isopycnals associated with Subantarctic and Subtropical Mode Water (26.5–26.8) and weaker water column stability in the upper thermocline. This same inter-basin difference in isopycnal depth and water column stability could partly explain why upwelling of PO_4 in the equatorial Pacific is a more important nutrient source than in the equatorial Atlantic basins. The nutrient supply situation in the S. Indian Ocean is closer to that in the S. Atlantic than S. Pacific oceans (Table 1).

The OM export rate is fairly consistent (1.9–2.8 mol C/m²/yr) between four of the five major ocean subbasins with the exception being the S. Indian ocean (Table 1). The low OM export rate in the S. Indian Ocean, in part, appears to be a result of stronger nutrient limitation on P utilization. The subtropical gyres represent the final stop on the nutrient supply train. If all the PO_4 within the gyres were consumed, then the global OM export would depend only on the rate of dissolved PO_4 supply. For the subtropical gyres in the N. Atlantic and N. Pacific Oceans where nearly all the PO_4 is utilized, the OM export rate would increase by <5% if all remaining PO_4 was consumed, whereas in the subtropical S. Indian Ocean OM export would double. Thus, the observed inter-basin variations of OM export depend on the interplay between physical processes controlling dissolved nutrient supply and biological processes controlling nutrient uptake. Any alteration in these processes induced by climate change either in the past or future will modify the overall strength and regional variations of the ocean's biological pump.

Data Availability Statement

The climatological distributions of O_2 supersaturation state are available at the World Ocean Atlas data site at https://www.ncei.noaa.gov/data/oceans/woa/WOA18/DATA/. $^{13}C/^{12}C$ of DIC and phosphate data are available at the GLODAP data site https://www.glodap.info/. Low-level PO_4 data are available at

https://www.bco-dmo.org/dataset/764704/data. Dissolved organic phosphate concentrations are available at https://www.bco-dmo.org/dataset/855139. Drifter-based surface velocities are available at https://www.aoml.noaa.gov/phod/gdp/mean_velocity.php. The ARGO mixed layer depths are available at http://www.argo.ucsd.edu. The CCMP wind speeds are available at http://apdrc.soest.hawaii.edu/datadoc/ccmp_month.php.

References

Abell, J., Emerson, S., & Renaud, P. (2000). Distributions of TOP, TON, and TOC in the North Pacific subtropical gyre: Implications for nutrient supply in the surface ocean and remineralization in the upper thermocline. *Journal of Marine Research*, *58*(2), 203–222. https://doi.org/10.1357/002224000321511142

Arteaga, L. A., Pahlow, M., Bushinsky, S. M., & Sarmiento, J. L. (2019). Nutrient controls on export production in the Southern Ocean. *Global Biogeochemical Cycles*, *33*(8), 942–956. https://doi.org/10.1029/2019GB006236

Atlas, R., Hoffman, R. N., Ardizzone, J., Leidner, S. M., Jusem, J. C., Smith, D. K., & Gombos, D. (2011). A cross-calibrated, multiplatform ocean surface wind velocity product for meteorological and oceanographic applications [Dataset]. *Bulletin America Meteorology Social*, *92*, 157–174. https://doi.org/10.1175/2010BAMS2946.1

Ayers, J. M., Strutton, P. G., Coles, V. J., Hood, R. R., & Matear, R. J. (2014). Indonesian throughflow nutrient fluxes and their potential impact on Indian Ocean productivity. *Geophysical Research Letters*, *41*(14), 5060–5067. https://doi.org/10.1002/2014GL060593

Billheimer, S. J., Talley, L. D., & Martz, T. R. (2021). Oxygen seasonality, utilization rate, and impacts of vertical mixing in the Eighteen Degree Water region of the Sargasso Sea as observed by profiling biogeochemical floats. *Global Biogeochemical Cycles*, *35*(3), e2020GB006824. https://doi.org/10.1029/2020GB006824

Bisson, K. M., Siegel, D. A., DeVries, T., Cael, B. B., & Buesseler, K. O. (2018). How data set characteristics influence ocean carbon export models. *Global Biogeochemical Cycles*, *32*(9), 1312–1328. https://doi.org/10.1029/2018GB005934

Bopp, L., Monfray, P., Aumont, O., Dufresne, J.-L., Le Treut, H., Madec, G., et al. (2001). Potential impact of climate change on marine export production. *Global Biogeochemical Cycles*, *15*(1), 81–99. https://doi.org/10.1029/1999gb001256

Boyd, P. W., Jickells, T., Law, C. S., Blain, S., Boyle, E. A., Buesseler, K. O., et al. (2007). Mesoscale iron enrichment experiments 1993–2005: Synthesis and future directions. *Science*, *315*(5812), 612–617. https://doi.org/10.1126/Science.1131669

Boyd, P. W., & Trull, T. W. (2007). Understanding the export of marine biogenic particles: Is there consensus? *Progress in Oceanography*, *72*(4), 276–312. https://doi.org/10.1016/j.pocean.2006.10.007

Boyer, T. P., Garcia, H. E., Locarnini, R. A., Zweng, M. M., Mishonov, A. V., Reagan, J. R., et al. (2018). World Ocean Atlas 2018 [Dataset]. NOAA National Centers for Environmental Information. https://www.ncei.noaa.gov/data/oceans/woa/WOA18/DATA/

Bushinsky, S. M., & Emerson, S. (2015). Marine biological production from in situ oxygen measurements on a profiling float in the subarctic Pacific Ocean. *Global Biogeochemical Cycles*, *29*(12), 2050–2060. https://doi.org/10.1002/2015GB005251

DeVries, T., & Weber, T. (2017). The export and fate of organic matter in the ocean: New constraints from combining satellite and oceanographic tracer observations. *Global Biogeochemical Cycles*, *31*(3), 31–555. https://doi.org/10.1002/2016GB005551

Dunne, J. P., Sarmiento, J. L., & Gnanadesikan, A. (2007). A synthesis of global particle export from the surface ocean and cycling through the ocean interior and on the seafloor. *Global Biogeochemical Cycles*, *21*(4), GB4006. https://doi.org/10.1029/2006GB002907

Emerson, S. (2014). Annual net community production and the biological carbon flux in the ocean. *Global Biogeochemical Cycles*, *28*(1), 14–28. https://doi.org/10.1002/2013gb004680

Fassbender, A. J., Sabine, C. L., & Cronin, M. F. (2016). Net community production and calcification from 7 years of NOAA Station Papa Mooring measurements. *Global Biogeochemical Cycles*, *30*(2), 250–267. https://doi.org/10.1002/2015gb005205

Fawcett, S. E., Johnson, K. S., Riser, S. C., Van Oostende, N., & Sigman, D. M. (2018). Low-nutrient organic matter in the Sargasso Sea thermocline: A hypothesis for its role, identity, and carbon cycle implications. *Marine Chemistry*, *207*, 108–123. https://doi.org/10.1016/j.marchem.2018.10.008

Goericke, R., & Fry, B. (1994). Variations of marine plankton $\delta^{13}C$ with latitude, temperature, and dissolved CO_2 in the world ocean. *Global Biogeochemical Cycles*, *8*(1), 85–90. https://doi.org/10.1029/93GB03272

Goodman, P. J., Hazeleger, W., de Vries, P., & Cane, M. (2005). Pathways into the Pacific equatorial undercurrent: A trajectory analysis. *Journal of Physical Oceanography*, *35*(11), 2134–2151. https://doi.org/10.1175/JPO2825.1

Gruber, N., Bates, N., & Keeling, C. D. (2002). Interannual variability in the North Atlantic carbon sink. *Science*, *298*(5602), 2374–2378. https://doi.org/10.1126/science.1077077

Hansell, D. A., & Carlson, C. A. (2001). Biogeochemistry of total organic carbon and nitrogen in the Sargasso Sea: Control by convective overturn. *Deep-Sea Research II*, *48*(8–9), 1649–1667. https://doi.org/10.1016/s0967-0645(00)00153-3

Haskell, W. Z., II., Fassbender, A. J., Long, J. S., & Plant, J. N. (2020). Annual net community production of particulate and dissolved organic carbon from a decade of biogeochemical profiling float observations in the Northeast Pacific. *Global Biogeochemical Cycles*, *34*(10), e2020GB006599. https://doi.org/10.1029/2020GB006599

Hedges, J. I., Baldock, J. A., Gelinas, Y., Lee, C., Peterson, M. L., & Wakeham, S. G. (2002). The biochemical and elemental compositions of marine plankton: A NMR perspective. *Marine Chemistry*, *78*(1), 47–63. https://doi.org/10.1016/s0304-4203(02)00009-9

Holte, J., Talley, L. D., Gilson, J., & Roemmich, D. (2017). An Argo mixed layer climatology and database. [Dataset]. Geophysical Research Letters, *44*, 5618–5626. https://doi.org/10.1002/2017GL073426

Hopkinson, C. S., & Vallino, J. J. (2005). Efficient export of carbon to the deep ocean through dissolved organic matter. *Nature*, *433*(7022), 142–145. https://doi.org/10.1038/nature03191

Jenkins, W. J., & Doney, S. C. (2003). The subtropical nutrient spiral. *Global Biogeochemical Cycles*, *17*(4), 1110. https://doi.org/10.1029/2003GB002085

Johnson, G. C., McPhaden, M. J., & Firing, E. (2001). Equatorial Pacific Ocean horizontal velocity, divergence, and upwelling. *Journal of Physical Oceanography*, *31*(3), 839–850. https://doi.org/10.1175/1520-0485(2001)031<0839:epohvd>2.0.co;2

Johnson, K. S., Riser, S. C., & Karl, D. M. (2010). Nitrate supply from deep to near-surface waters of the North Pacific subtropical gyre. *Nature*, *465*(7301), 1062–1065. https://doi.org/10.1038/nature09170

Key, R. M., Olsen, A., van Heuven, S., Lauvset, S. K., Velo, A., Lin, X., et al. (2015). Global Ocean data analysis project, version 2 (GLODAPv2). ORNL/CDIAC-162, NDP-093. *Carbon dioxide information analysis center* [Dataset]. Oak Ridge National Laboratory, US Department of Energy. https://doi.org/10.3334/CDIAC/OTG.NDP093_GLODAPv2

Knapp, A. N., Letscher, R. T., & Liang, Z. (2021). DOP concentration observations from the global ocean between 1990 and 2021 (DOP N2 fixation and export production project) (Version 1) Version Date 2021-10-05. [Dataset]. Biological and Chemical Oceanography Data Management Office (BCO-DMO). https://doi.org/10.26008/1912/bco-dmo.855139.1

Körtzinger, A., Send, U., Lampitt, R. S., Hartman, S., Wallace, D. W. R., Karstensen, J., et al. (2008). The seasonal pCO2 cycle at 49°N/16.5°W in the northeastern Atlantic Ocean and what it tells us about biological productivity. *Journal of Geophysical Research*, *113*(C4), C04020. https://doi.org/10.1029/2007JC004347

Laufkötter, C., Vogt, M., & Gruber, N. (2013). Long-term trends in ocean plankton production and particle export between 1960 and 2006. *Biogeosciences*, *10*(11), 7373–7393. https://doi.org/10.5194/bg-10-7373-2013

Laufkötter, C., Vogt, M., Gruber, N., Aumont, O., Bopp, L., Doney, S. C., et al. (2016). Projected decreases in future marine export production: The role of the carbon flux through the upper ocean ecosystem. *Biogeosciences*, *13*, 4023–4047. https://doi.org/10.5194/bg-13-4023-2016

Laurindo, L., Mariano, A., & Lumpkin, R. (2017). An improved near-surface velocity climatology for the global ocean from drifter observations [Dataset]. Deep-Sea Research I, *124*, 73–92. https://doi.org/10.1016/j.dsr.2017.04.009

Lauvset, S. K., Key, R. M., Olsen, A., van Heuven, S., Velo, A., Lin, X., et al. (2016). A new global interior ocean mapped climatology: The 1°x1° GLODAP version 2 [Dataset]. Earth System Science Data, *8*, 325–340. https://doi.org/10.5194/essd-8-325-2016

Laws, E. A., D'Sa, E., & Naik, P. (2011). Simple equations to estimate ratios of new or export production to total production from satellite-derived estimates of sea surface temperature and primary production. *Limnology and Oceanography: Methods*, *9*(12), 593–601. https://doi.org/10.4319/lom.2011.9.593

Letscher, R. T., Primeau, F., & Moore, J. K. (2016). Nutrient budgets in the subtropical ocean gyres dominated by lateral transport. *Nature Geoscience*, *9*(11), 815–819. https://doi.org/10.1038/NGEO2812

Li, Z., & Cassar, N. (2016). Satellite estimates of net community production based on O2/Ar observations and comparison to other estimates. *Global Biogeochemical Cycles*, *30*(5), 735–752. https://doi.org/10.1002/2015gb005314

Liao, F., Liang, X., Li, Y., & Spall, M. (2022). Hidden upwelling systems associated with major Western boundary currents. *Journal of Geophysical Research: Oceans*, *127*(3), e2021JC017649. https://doi.org/10.1029/2021JC017649

Mahadevan, A. (2016). The impact of submesoscale physics on primary productivity of plankton. *Annual Review of Marine Science*, *8*(1), 161–184. https://doi.org/10.1146/annurev-marine-010814-015912

Mahaffey, C., Williams, R. G., Wolff, G. A., & Anderson, W. T. (2004). Physical supply of nitrogen to phytoplankton in the Atlantic Ocean. *Global Biogeochemical Cycles*, *18*(1), GB1034. https://doi.org/10.1029/2003GB002129

Martiny, A., Lomas, M. W., Fu, W., Boyd, P. W., Chen, Y. l. L., Cutter, G. A., et al. (2019). Biogeochemical controls of surface ocean phosphate [Dataset]. Science Advances, *5*, eaax0341. https://doi.org/10.1126/sciadv.aax0341

Martiny, A. C., Pham, C. T. A., Primeau, F. W., Vrugt, J. A., Moore, J. K., Levin, S. A., & Lomas, M. W. (2013). Strong latitudinal patterns in the elemental ratios of marine plankton and organic matter. *Nature Geoscience*, *6*(4), 279–283. https://doi.org/10.1038/ngeo1757

Mather, R. L., Reynolds, S. E., Wolff, G. A., Williams, R. G., Torres-Valdes, S., Pan, X., et al. (2008). Contrasting phosphorus cycling in Atlantic Ocean deserts. *Nature Geoscience*, *1*(7), 439–443. https://doi.org/10.1038/ngeo232

McGillicuddy, D., Anderson, L. A., Bates, N. R., Bibby, T., Buesseler, K. O., Carlson, C. A., et al. (2007). Eddy/wind interactions stimulate extraordinary mid-ocean plankton blooms. *Science*, *316*(5827), 1021–1026. https://doi.org/10.1126/science.1136256

Mills, M. M., Ridame, C., Davey, M., La Roche, J., & Geider, R. J. (2004). Iron and phosphorus co-limit N fixation in the eastern tropical North Atlantic. *Nature*, *429*(6989), 292–294. https://doi.org/10.1038/nature02550

Najjar, R. G., Jin, X., Louanchi, F., Aumont, O., Caldeira, K., Doney, S. C., et al. (2007). Impact of circulation on export production, dissolved organic matter, and dissolved oxygen in the ocean: Results from phase II of the ocean carbon-cycle model intercomparison project (OCMIP-2). *Global Biogeochemical Cycles*, *21*(3), GB3007. https://doi.org/10.1029/2006GB002857

Neuer, S., Cianca, A., Helmke, P., Freudenthal, T., Davenport, R., Meggers, H., et al. (2007). Biogeochemistry and hydrography in the eastern subtropical North Atlantic gyre. Results from the European time-series station ESTOC. *Progress in Oceanography*, *72*, 1–29. https://doi.org/10.1016/j.pocean.2006.08.001

Osborn, T. R. (1980). Estimates of the local rate of vertical diffusion from dissipation measurements. *Journal of Physical Oceanography*, *10*(1), 83–89. https://doi.org/10.1175/1520-0485(1980)010<0083:eotlro>2.0.co;2

Oschlies, A., & Garcon, V. (1998). Eddy-induced enhancement of primary production in a model of the North Atlantic Ocean. *Nature*, *394*(6690), 266–269. https://doi.org/10.1038/28373

Ostle, C., Johnson, M., Landschutzer, P., Schuster, U., Hartman, S., Hull, T., & Robinson, C. (2015). Net community production in the North Atlantic Ocean derived from volunteer observing ship data. *Global Biogeochemical Cycles*, *29*(1), 80–95. https://doi.org/10.1002/2014gb004868

Palevsky, H. I., & Doney, S. C. (2018). How choice of depth horizon influences the estimated spatial patterns and global magnitude of ocean carbon export flux. *Geophysical Research Letters*, *45*(9), 4171–4179. https://doi.org/10.1029/2017gl076498

Palevsky, H. I., & Quay, P. D. (2017). Influence of biological carbon export on ocean carbon uptake over the annual cycle across the North Pacific Ocean. *Global Biogeochemical Cycles*, *31*(1), 81–95. https://doi.org/10.1002/2016GB005527

Palevsky, H. I., Quay, P. D., Lockwood, D. E., & Nicholson, D. P. (2016). The annual cycle of gross primary production, net community production, and export efficiency across the North Pacific Ocean. *Global Biogeochemical Cycles*, *30*(2), 361–380. https://doi.org/10.1002/2015gb005318

Primeau, F. W., Holzer, M., & DeVries, T. (2013). Southern Ocean nutrient trapping and the efficiency of the biological pump. *Journal of Geophysical Research: Oceans*, *118*(5), 2547–2564. https://doi.org/10.1002/jgrc.20181

Quay, P., Emerson, S., & Palevsky, H. (2020). Regional pattern of the ocean's biological pump based on geochemical observations. *Geophysical Research Letters*, *47*(14), e2020GL088098. https://doi.org/10.1029/2020GL088098

Quay, P., Sonnerup, R., Munro, D., & Sweeney, C. (2017). Anthropogenic CO$_2$ accumulation and uptake rates in the Pacific Ocean based on changes in the ^{13}C/^{12}C of dissolved inorganic carbon. *Global Biogeochemical Cycles*, *31*(1), 59–80. https://doi.org/10.1002/2016GB005460

Quay, P. D., Stutsman, J., Feely, R. A., & Juranek, L. W. (2009). Net community production rates across the subtropical and equatorial Pacific Ocean estimated from air-sea δ^{13}C disequilibrium. *Global Biogeochemical Cycles*, *23*(2), GB2006. https://doi.org/10.1029/2008GB003193

Redfield, A. C. (1958). The biological control of chemical factors in the environment. *American Scientist*, *46*, 205–221.

Reynolds, S., Mahaffey, C., Roussenov, V., & Williams, R. G. (2014). Evidence for production and lateral transport of dissolved organic phosphorus in the eastern subtropical North Atlantic. *Global Biogeochemical Cycles*, *28*(8), 805–824. https://doi.org/10.1002/2013GB004801

Roach, C. J., Balwada, D., & Speer, K. (2018). Global observations of horizontal mixing from Argo float and surface drifter trajectories. *Journal of Geophysical Research: Oceans*, *123*(7), 4560–4575. https://doi.org/10.1029/2018JC013750

Sarmiento, J. L., Gruber, N., Brzezinski, M. A., & Dunne, J. P. (2004). High-latitude controls of thermocline nutrients and low latitude biological productivity. *Nature*, *427*(6969), 56–60. https://doi.org/10.1038/nature02127

Schlitzer, R. (2002). Carbon export fluxes in the southern ocean: Results from inverse modeling and comparison with satellite-based estimates. *Deep-Sea Research, Part II*, *49*(9), 1623–1644. https://doi.org/10.1016/s0967-0645(02)00004-8

Siegel, D. A., Buesseler, K. O., Doney, S. C., Sailley, S. F., Behrenfeld, M. J., & Boyd, P. W. (2014). Global assessment of ocean carbon export by combining satellite observations and food-web models. *Global Biogeochemical Cycles*, *28*(3), 181–196. https://doi.org/10.1002/2013gb004743

Sonnerup, R. E., Mecking, S., Bullister, J. L., & Warner, M. J. (2015). Transit time distributions and oxygen utilization rates from chlorofluorocarbons and sulfur hexafluoride in the Southeast Pacific Ocean. *Journal of Geophysical Research: Oceans*, *120*(5), 3761–3776. https://doi.org/10.1002/2015jc010781

Sonnerup, R. E., Quay, P. D., & Bullister, J. L. (1999). Thermocline ventilation and oxygen utilization rates in the subtropical North Pacific based on CFC distributions during WOCE. *Deep-Sea Research, Part A: Oceanographic Research Papers I*, *46*(5), 777–805. https://doi.org/10.1016/s0967-0637(98)00092-2

Steinberg, D. K., & Landry, M. R. (2017). Zooplankton and the Ocean carbon cycle. *Annual Review of Marine Science*, *9*(1), 413–444. https://doi.org/10.1146/annurev-marine-010814-015924

Takahashi, T., Sutherland, S. C., Wanninkhof, R., Sweeney, C., Feely, R. A., Chipman, D. W., et al. (2009). Climatological mean and decadal change in surface ocean pCO2, and net sea-air CO_2 flux over the global oceans. *Deep Sea Research II*, *56*(8–10), 554–577. https://doi.org/10.1016/j.dsr2.2008.12.009

Tanioka, T., & Matsumoto, K. (2017). Buffering of ocean export production by flexible elemental stoichiometry of particulate organic matter. *Global Biogeochemical Cycles*, *31*(10), 1528–1542. https://doi.org/10.1002/2017GB005670

Tsuchiya, M., & Talley, L. D. (1998). A Pacific hydrographic section at 88°W: Water-property distribution. *Journal of Geophysical Research*, *03*(C6), 12899–12918. https://doi.org/10.1029/97jc03415

Wanninkhof, R. (2014). Relationship between wind speed and gas exchange over the ocean revisited. *Limnology and Oceanography: Methods*, *12*(6), 351–362. https://doi.org/10.4319/lom.2014.12.351

Williams, R. G., & Follows, M. J. (1998). The Ekman transfer of nutrients and maintenance of new production over the North Atlantic. *Deep Sea Research Part I: Oceanographic Research Papers*, *45*(2–3), 461–489. https://doi.org/10.1016/S0967-0637(97)00094-0

Williams, R. G., Roussenov, V., & Follows, M. J. (2006). Nutrient streams and their induction into the mixed layer. *Global Biogeochemical Cycles*, *20*(1), gb1016. https://doi.org/10.1029/2005gb002586

Yang, B., Emerson, S. R., & Bushinsky, S. M. (2017). Annual net community production in the subtropical Pacific Ocean from in situ oxygen measurements on profiling floats. *Global Biogeochemical Cycles*, *31*(4), 728–744. https://doi.org/10.1002/2016GB005545

Yang, B., Emerson, S. R., & Quay, P. (2019). The subtropical ocean's biological carbon pump determined from O_2 and DIC/DI^{13}C tracers. *Geophysical Research Letters*, *46*(10), 5361–5368. https://doi.org/10.1029/2018GL081239

Zhang, J., & Quay, P. D. (1997). The total organic carbon export rate based on DIC and DIC13 budgets in the equatorial Pacific Ocean. *Deep-Sea Research II*, *44*(9–10), 2163–2190. https://doi.org/10.1016/s0967-0645(97)00032-5